DOI: 10.1002/cphc.201100158

Terahertz Time-Domain Spectroscopy of Gases, Liquids, and Solids

Michael Theuer,*[a, b] Srikantaiah Sree Harsha,[c] Daniel Molter,[a] Garik Torosyan,[b] and René Beigang[a, b]

The techniques and methods employed in the spectroscopic characterization of gases, liquids, and solids in the terahertz frequency range are reviewed. Terahertz time-domain spectroscopy is applied to address a broadband frequency range between 100 GHz and 5 THz with a sub-10 GHz frequency resolution. The unique spectral absorption features measured can be efficiently used in material identification and sensing. Possibilities and limitations of fundamental and industrial applications are discussed.

1. Introduction

Various frequency ranges of the electromagnetic spectrum are used for the investigation of material properties, from high-energy X-rays to long-wavelength microwaves. For spectroscopic identification, infrared (IR) radiation is especially well established due to its high selectivity and fingerprint-like absorption signatures. Sandwiched between the microwave and IR bands, the terahertz (THz) frequency band is known to exhibit properties and phenomena observed in both the neighboring regions. This band covers frequencies between 100 GHz and 10 THz, which corresponds to vacuum wavelengths between 3 mm and 30 μm (see electromagnetic spectrum in Figure 1).

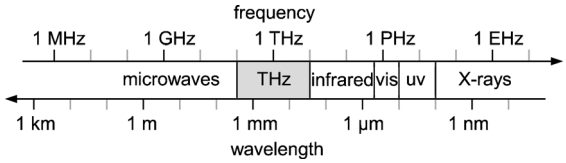

Figure 1. Location of the terahertz (THz) frequency range in the electromagnetic spectrum. In free space, a frequency of 1 THz corresponds to a wavelength of 300 μm or to 33.3 wavenumbers.

The IR activity associated with molecular transitions and the dielectric transparency characteristic of microwaves are seen even in the THz region. So in the THz frequency window it is possible to have a reasonable penetration depth, along with the expression of significant characteristic absorption features. These advantages are explored for various fundamental and industrial applications.[1]

In the past, this frequency range, formally also known as the far-infrared, was rarely used because of lack of powerful transmitters and sensitive receivers. With the ongoing development of laser sources, a lot of new possibilities arose leading to coherent and incoherent THz systems. There are THz laser sources, based either on direct transitions in molecular gases (e.g., methanol[2]) or on interband transitions in quantum cascade lasers.[3] In the photonic approach, there are for example two-color mixed continuous-wave (cw) systems,[4] where the beat frequency between two colors is in the THz frequency range. Also, parametric processes excited by nanosecond pulses have been reported.[5,6] With near-IR femtosecond pump pulses, either optical rectification or transient photoconductivity is used to generate THz radiation.[7] Further, based on an electronic approach (e.g., frequency-modulated continuous waves[8]), other types of systems are reported, each with their individual advantages and limitations.

In this Minireview, we will concentrate on THz systems that are suited for broadband spectroscopy. Therefore, the principle of THz time-domain spectroscopy (THz-TDS) is applied.[9] It is based on the coherent generation and detection of pulsed THz radiation using components gated by femtosecond laser pulses. A frequency of 1 THz corresponds to a cycle duration of 1 ps, which means that THz frequencies are located at the very limits of the frequency response of electronic devices. With typical commercial titanium:sapphire or recently developed fiber lasers (100 fs pulse duration), frequencies between 100 GHz and 5 THz can be detected.

Since no electronic device or amplifier can so far directly respond to the high-frequency oscillations of the THz electric field, there is an urgent need to reduce the required high-fre-

[a] *Dr. M. Theuer, D. Molter, Prof. Dr. R. Beigang*
Department of Physics and Research Center OPTIMAS
University of Kaiserslautern
67663 Kaiserslautern (Germany)
Fax: (+49) 631-205-5102
E-mail: theuer@physik.uni-kl.de
Homepage: http://www.physik.uni-kl.de/beigang

[b] *Dr. M. Theuer, Dr. G. Torosyan, Prof. Dr. R. Beigang*
Department of Terahertz Measurement and Systems
Fraunhofer Institute for Physical Measurement Techniques IPM
67663 Kaiserslautern (Germany)

[c] *S. S. Harsha*
School of Electrical & Computer Engineering
Oklahoma State University
Stillwater, OK 74078 (USA)

 © 2011 Wiley-VCH Verlag GmbH & Co. KGaA, Weinheim

quency response of the detection scheme. Other optomechanical techniques need to be employed to detect the fast oscillation. This is done by using THz-TDS to sample the electric field slowly (for the setup, see Figure 2). A beam splitter separates

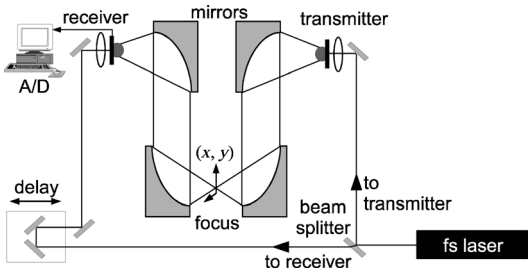

Figure 2. Sketch of a terahertz time-domain spectroscopy (THz-TDS) system.

two fractions of the same laser pulse, one for the transmitter and one for the receiver arm. Comparable to a pump–probe experiment, only the relative delay between generation and detection laser pulses has to be taken into account. A mechanical movement of a stepper-motor-driven linear stage changes the path length of the receiver arm by moving a retro reflective mirror. If the stepper motor is standing still, it is a quasi-DC case for the connected electronics. For the detection of the transmitted THz waves, the high frequencies are only present in the receiving chip itself (carrier lifetimes below 1 ps). Then the integrating window of the laser pulse is shifted to sample the electric field of the THz pulse using electronic components with a kilohertz frequency response.

In contrast to intensity measurements (e.g., power meters or standard FTIR spectroscopy), THz-TDS allows recording of the electric field E directly and not just the intensity. An intensity measurement $I \propto |E|^2$ would lose the entire phase information. Applying THz-TDS, the signed digitized electric field $E(t)$ is sampled in the time domain as a function of the delay t. A Fourier transformation connects the quantity in the time domain to an equivalent complex quantity in the frequency domain $\tilde{E}(\omega)$.

Consider a broadband THz pulse $\tilde{E}(\omega)_{in}$ propagating through a medium of length l, then the amplitude and the phase of the pulse will be changed according to Equation (1):[10]

$$\tilde{E}(\omega)_{out} = \tilde{E}(\omega)_{in} e^{i\tilde{k}(\omega)l} \quad (1)$$

with $\tilde{k}$ the complex wave vector consisting of a real part, describing the propagation in space, and an imaginary part corresponding to the material absorption. Decomposition gives Equation (2):

$$\tilde{k}(\omega) = k_0 + \Delta k(\omega) + i\frac{\alpha(\omega)}{2} \quad (2)$$

with k_0 the constant wave vector given by the classic refractive index, $\Delta k(\omega)$ describing phase-dependent effects such as dispersion, and $\alpha(\omega)$ the absorption coefficient. If now the spectral amplitude of a measurement is divided by that of a reference, the amplitude transmission containing the amplitude and phase information can be derived [Eq. (3)]:

$$t = \frac{\tilde{E}(\omega)_{sample}}{\tilde{E}(\omega)_{reference}} = e^{-\alpha(\omega)l/2} e^{i[k_0 + \Delta k(\omega)]l} \quad (3)$$

In an intensity transmission measurement [Eq. (4)]:

$$T = |t|^2 = \frac{I(\omega)_{sample}}{I(\omega)_{reference}} = e^{-\alpha(\omega)l} \quad (4)$$

the phase information is lost.

The key components required to achieve a good performance (broadband pulses, high peak power, low noise level) are the transmitters and the receivers. In our system we apply photoconductive antennae as high-frequency components.[11] Both the transmitter and receiver are identical chips, but operated in different electronic modes (see Figure 3). The devices

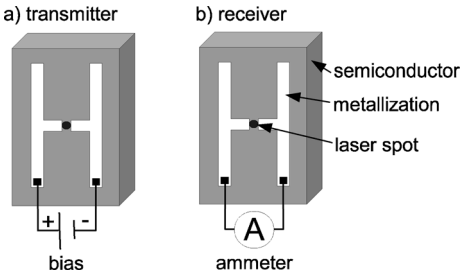

Figure 3. Layout of a photoconductive switch consisting of an illuminated dipole antenna on a semiconductor substrate. a) In the transmitter, the external bias accelerates the free charge carriers. b) In the receiver, the THz electric field drives the current in the antenna.

are processed onto a low-temperature grown gallium arsenide layer deposited on a gallium arsenide substrate. This is the active area with a very short carrier lifetime (below 1 ps). A conductive metal is deposited forming a Hertzian dipole as a resonant structure. This is an H-shaped form with a gap in the center, like a "broken" antenna. In the dark (unilluminated) state, the semiconductor (antenna) shows a high resistivity due to the absence of free carriers. Typical resistivities for a gap width of 5 μm are in the megaohm range. If now photons get absorbed in the gap, electron–hole pairs are generated which can move freely in an external field. So the resistivity drops down to the kiloohm range and the antenna becomes "conductive".

Driving this chip as a transmitter, an external electric bias (≈50 V) is applied to the antenna (typically resulting in a field strength of 10 kV mm^{-1}). If now the laser pulse shorts the antenna, the excited electrons are accelerated and a large current transient occurs. During this short period the Hertzian dipole emits THz radiation. Turning off the illumination (end of the laser pulse) and after the recombination time of charge carriers (lifetime of the semiconductor), the resistivity increases again and the current breaks down. Depending on the particular shape of the antenna, different frequencies can be generated more efficiently or special beam profiles can be designed. Be-

 © 2011 Wiley-VCH Verlag GmbH & Co. KGaA, Weinheim

sides the dipole antennae, also strip-line, bow-tie, or meander geometries are used.[12]

Operating the chip as a receiver, the THz field guided by the THz optics from the transmitter accelerates the generated electrons. This is only possible if the THz field coincides with the laser pulse illumination driving a current in the antenna. This current is directly proportional to the THz electric field. Before A/D conversion the signal is amplified in a transimpedance amplifier and measured in a lock-in amplifier. The antenna produces a signal only if the THz pulse and the laser pulse are incident at the same time. This results in a high signal-to-noise ratio (SNR) for the detection mechanism. The ratio between the durations of sensitive period and the dark state is called the duty cycle. For a pump laser with a pulse duration of 100 fs at a repetition rate of 100 MHz the duty cycle is 10^{-5}. This is advantageous as during the off time of the detector no further noise is integrated in the absence of THz radiation.

The coupling and guiding of THz waves follows the rules of quasi-optics.[9] Regarding the beam path in Figure 2, the THz waves are emitted from a photoconductive dipole antenna linearly polarized in plane. Silicon lenses attached to the transmitter and receiver chips collimate the beam. A wavelength-dependent Gaussian beam with a diameter of approximately 1 cm is formed after the first off-axis parabolic mirror. The spot diameter is wavelength dependent with the short wavelengths closer to the center axis. Four metal mirrors are used to allow measurements with either a collimated or focused beam. A wavelength-dependent focus with typically 1 mm diameter can be obtained.[12] The incident THz radiation is focused again into the detector by using a silicon lens. As already described, the electric field drives a current in the receiver.

Various types of emitters (photoconductive surface emitters,[13,14] nonlinear sources based on optical rectification or difference frequency generation)[15,16] or detectors (photoconductive antennae,[7] electro-optic crystals[17]) can be used with femtosecond-laser-pumped systems. But photoconductive antennae have proven to show a very good performance in terms of SNR and bandwidth at low laser power consumption. That also allows fiber-guided pump beam delivery to the transmitter and receiver.[18]

The average THz power of this femtosecond-laser-pumped THz system is typically very low (less than 1 μW) compared to other sources, such as microwave oscillators or direct lasers. Moreover, THz radiation has photon energies in the milli electron volt range and hence is nonionizing. This has the advantage that there is no health risk related to the application of femtosecond THz radiation, neither for the measured object nor the human operator. On the other hand, the coherent detection of the electric field offers a high brightness in terms of SNR, which makes this approach superior to incoherent detectors such as bolometers or pyroelectric detectors. Also the thermal background and electromagnetic noise can be filtered out very efficiently in this coherent detection scheme, thus enabling even measurements within hot flames.[19]

2. Gases

Many polar gases show narrowband absorption features in the THz range caused by rotational transitions.[20] This fact can be used for trace gas detection, but also causes problems for free-space measurement of THz transients in ambient air.[21] As water molecules are polar, absorption lines of water vapor are seen in the measurement even without inserted sample. In Figure 4 this is exemplarily shown for a 50-cm-long free-space

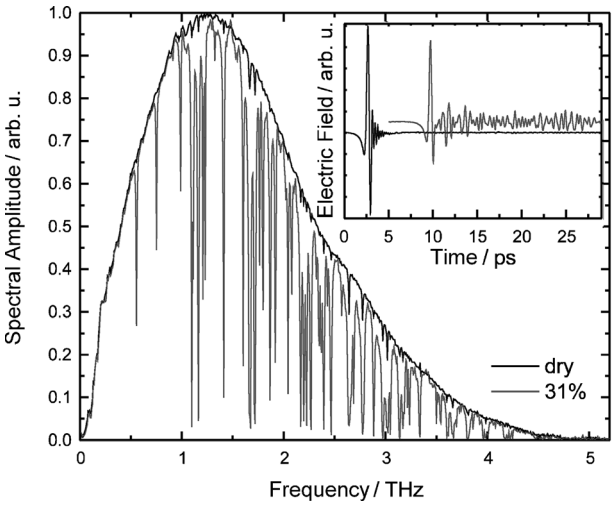

Figure 4. Influence of humidity in ambient air on the THz spectrum. Narrowband absorption lines caused by rotation modes of water molecules are seen in the frequency domain. Inset: Raw data acquired in the time domain (black: dry air reference; gray: 31% humidity).

propagation in dry air in comparison to standard laboratory atmosphere (31% humidity). In the inset the recorded raw data in the time domain are shown. The black line is the dry air reference. It is a sub-1 ps single-cycle pulse without any ringing or echo modulations afterwards. The Fourier transformation gives the spectral information (amplitude and phase). The spectral amplitude is plotted in Figure 4. It extends from 100 GHz to 4.5 THz with a maximum at 1.2 THz. The SNR is frequency dependent and typically better than 1000:1 at the maximum frequency. Tiny dips due to the residual humidity in the dry air can still be seen in the reference spectrum even if the system housing is completely purged.

If now air moisture is present in the path of the THz beam, the polar water molecules absorb a fraction of the THz intensity, which can be seen by the reduced peak amplitude in the time domain (Figure 4 inset, gray curve). After excitation of the dipoles, the molecules re-emit THz radiation. The superposition of the individual narrow lines gives rise to a strong modulation after the main peak. The Fourier transform shows a spectrum in which the particular frequencies are cut out. By dividing the recorded data by the reference in the frequency domain, the absorption coefficient can be calculated. So to investigate unknown samples, either the measurement chamber has to be purged with dry air or the water vapor absorption lines have to be removed numerically.

 © 2011 Wiley-VCH Verlag GmbH & Co. KGaA, Weinheim

Taking the data of Figure 4, which were recorded at 31% humidity and a cell length of 50 cm, the absorption coefficient for pure 100% humidity can be calculated. The plot in Figure 5 shows the results. Clearly distinct narrow absorption lines with

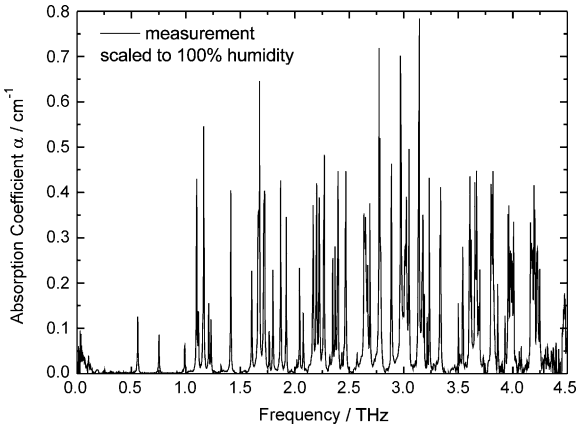

Figure 5. Measured absorption coefficient of water vapor. The recorded data of Figure 4 were used to calculate the absorption coefficient for 100% humidity.

a high absorption (some even stronger than 0.50 cm^{-1}) are present. A comparison with literature values[20] shows that here the calculated absorption coefficient is roughly 20% larger than expected. This can be caused by the inaccuracy of the hygrometer and the correct absorption length. But still, the relative absorption line strength is pretty accurate.

The fact that most polar molecules show rotational transitions in the THz frequency band is not only a limitation for THz standoff applications, but also can be used for sensing of gas molecules. Exemplarily, Figure 6 shows the measured absorption coefficient for carbon monoxide (CO) and nitric oxide (NO). Nearly a complete set of rotational transitions can be observed for both gases. Upon evaluating the measured center frequencies, a particular gas can be identified. The detection sensitivity is determined by the SNR of the system, the absorption coefficient of the sample, and the absorption length within the cell. Depending on these parameters, concentrations in the ppm range have been detected (for example, 300 ppm × m CO, 200 ppm × m NO, 20 ppm × m NH_3, 20 ppm × m HCl).[22] The most important line-broadening mechanism is pressure broadening. For example, when measuring the pressure-dependent linewidth of CO at 100 mbar, the linewidth is below 500 MHz, which is given by the spectrometer resolution. At 500 mbar, the lines are broadened to 2 GHz. Because of the narrow linewidth and the high resolution of the measurement, no cross sensitivity between different molecules has been observed so far. As a recent development, the technique of asynchronous optical sampling (ASOPS) is also applied in THz-TDS.[23] It is based on two high-repetition-rate femtosecond lasers, one to pump the transmitter and one to gate the detector. Their individual repetition rates are slightly detuned but stabilized. It allows for the fast scanning of transients (10 kHz typically) at a high spectral resolution (delay range up to 1 ns), which is of particular interest for online gas spectroscopy.[24,25]

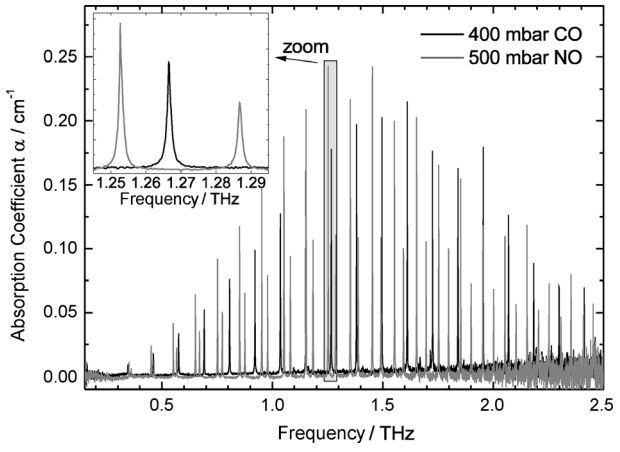

Figure 6. Measured absorption coefficient for carbon monoxide (CO) and nitric oxide (NO).[22]

3. Liquids

Unlike molecules in the gas phase, liquids in general do not have narrowband absorption features. The nonpolar liquids show a weak broadband absorption,[26] whereas polar liquids are strongly absorbing in the entire THz range.[27] Water, in particular, is nearly opaque in the THz range with an absorption dominated by intermolecular interactions due to permanent and induced dipole moments in the hydrogen-bonded network of water molecules.[28] Comparable to microwaves, a several tens of microns thick layer of water is sufficient to absorb most of the broadband THz intensity. The large absorption coefficient of water (absorption at 1 THz is $\alpha \approx 200\ cm^{-1}$) limits applications in biology in most instances where living cells are typically stored in an aqueous nutrient solution. Also in medicine, as the human body mostly consists of water, the penetration depth is too small to detect anything underneath the skin.[29] But the fact that THz radiation is strongly absorbed in water can also be used to design very sensitive moisture sensors.[1] For example, processes in paper manufacturing or corn milling require a very sensitive control of residual moisture in the product, which can be detected by using THz radiation.[30]

A demonstration of the THz peak reduction caused by moisture is given in Figure 7. It shows the transmitted amplitude through a sample of cocoa powder. The moisture was controlled by a climate chamber. The substance filled in an open container was placed for three days at 95% and afterwards at 0% humidity. The particular weights were measured and taken for a linear calibration of moisture content versus weight. A flat-pressed sample of roughly 25 g with a height of 3 mm was used to minimize the relative error of weight determination. Exposing the initially wet sample to dry air reduced the water content.

Clearly an exponentially decaying behavior of THz transmission as a function of moisture content in the powder is seen. So the transmitted THz amplitude can be taken as a quantity to determine the water content. Due to the material proper-

 © 2011 Wiley-VCH Verlag GmbH & Co. KGaA, Weinheim

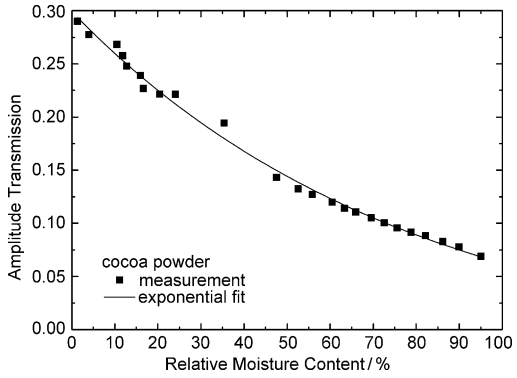

Figure 7. Moisture content in cocoa powder and its influence on the THz transmission.

ties, THz frequencies are the only ones that can perform such a measurement. Using IR radiation, the reduction of signal amplitude due to scattering in the fine powder would be too high. Even if the scattering losses depend on the grain size, THz radiation can penetrate the powder as the particle size is still smaller than the wavelength.

A spectral evaluation shows the superimposed influences of scattering at the grains and the absorption in water (Figure 8).

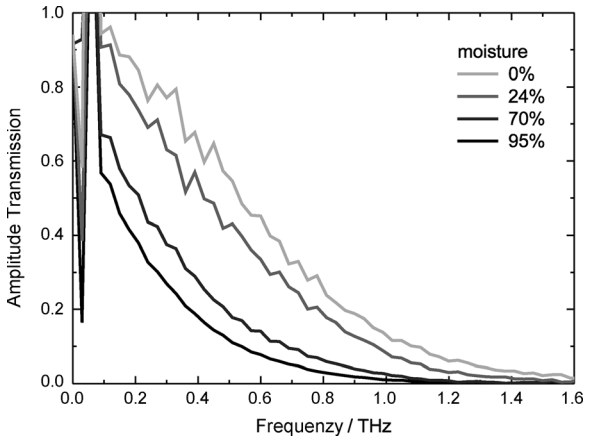

Figure 8. Spectral transmission of THz radiation through cocoa powder of different moisture contents. Constant influences of scattering (exponential decay) and reduced transmission due to water absorption (offset) are seen.

The exponential roll-off towards higher frequencies even at a completely dry sample is attributed to scattering. The reason is that the grain size is in the order of the wavelength, which leads to scattering losses. This limits the accessible frequencies to a maximum of approximately 1 THz, independent of the moisture content. Upon increasing the moisture content, the transmission is further reduced but without narrowband signatures. This is expected, as the absorption of liquid water is very broadband over the entire THz frequency band. So by choosing a fixed working frequency below 1 THz the transmission at a particular frequency could be monitored, which can also be done using a cw THz system.

In summary, the presence of water in the gas and especially in the liquid phase is one of the major limitations for THz spectroscopy. Transmission measurements of polar molecules are not possible in most instances or the absorption length has to be shortened significantly.[27] Another method to investigate polar liquids is to use the evanescent wave at an interface. This can be done by depositing a layer of liquid on a transparent mounting plate and investigating the reflection of the interface between mount and liquid.[28] According to Maxwell's equations and their boundary conditions for continuity, a fraction of the field leaks into the medium at the point of reflection. This fraction, called the evanescent wave, decays exponentially in space and interacts with the sample. So the reflected wave contains information on the second medium and is measured. This principle is called attenuated total reflection (ATR).[31] The major advantages are that the length of the effectively penetrated sample is rather short, which allows for the spectroscopy of very lossy samples, and that the sample height on top of the sensor has no influence on the measurement. The penetration depth is only tens of microns, which is much less than the sample thickness. If there is more sample on the sensor the measurement process is not influenced.

A more sophisticated arrangement uses the interface as a reflecting cavity mirror. So the evanescent wave and the liquid to be measured are within a resonator allowing more sensitive measurements. The corresponding setup (Figure 9) consists of

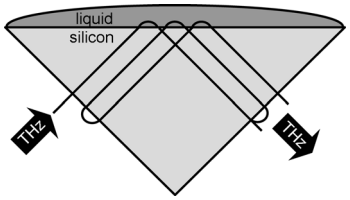

Figure 9. Setup of an attenuated total reflection (ATR) sensor. The evanescent wave at the point of total internal reflection interacts with the liquid sample.[32]

a prism-shaped monolithic Fabry–Perot resonator made of high-resistivity silicon.[32] The material itself is nearly lossless and has a high refractive index of 3.41. The angles are 45°× 90°×45° to have normal incidence at the entrance facet (left). Then the THz beam hits the measurement interface (top) at an angle larger than the critical angle of total internal reflection. The evanescent wave interacts with the liquid and propagates to the next prism facet (right). As a fraction of the intensity gets reflected at the silicon/air interface, the THz radiation bounces back and forth within the prism. At each round trip, the THz radiation interacts twice with the sample via the evanescent wave.

As no narrowband signatures are expected, this measurement was carried out with a cw electronic source (BWO, tunable around 600 GHz). For further experimental details, see Dobroiu et al.[32] The transmission through the entire device is recorded. The prism acts as a Fabry–Perot resonator with "internal" losses caused by absorption at the total reflection surface. The measured samples are ethanol solutions of varying con-

 © 2011 Wiley-VCH Verlag GmbH & Co. KGaA, Weinheim

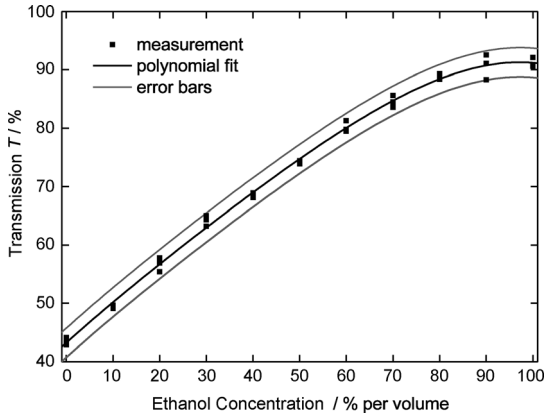

Figure 10. Measured THz transmission of the ATR sensor covered with ethanol solution of different concentration.[32]

centrations in water. As a result, the measured transmission (Figure 10) shows that the more water is present, the less transmission can be reached caused by the reduced finesse of the resonator. The two lines parallel to the curve correspond to an error bar obtained by reproducing the measurement series. This dependency can be used to calibrate the sensor. So when neglecting narrowband spectral features, measurement of polar liquids is also possible and concentrations can be determined.

4. Solids

Many crystalline molecules show vibrational phonon modes in the THz range. Unlike amorphous substances, crystalline samples have distinguishable absorption lines due to the low-frequency vibrational modes. Figure 11 shows the measured absorption coefficient of tartaric acid, sucrose, lactose and Teflon. All of these crystalline substances show absorption features in the THz range. For the measurement process the samples were prepared as diluted, 1.4-mm-thick pressed pellets. The matrix is either polyethylene or PTFE powder, which is inactive in the THz range. This guarantees a homogeneous sample with fewer scattering losses and allows for broadband data acquisition. The superimposed periodic modulation on all measured absorption coefficients is caused by an etalon effect within the sample. The THz pulse bounces back and forth in the weakly absorbing pellet, thereby giving rise to echo pulses after the main peak with a separation of 14 ps each. This echo corresponds to the observable modulation of 70 GHz in the spectra, which can be removed by standard software tools.

Detecting these features may be a potential application of THz radiation in the field of security applications, such as the detection of drugs[33] or explosives.[34] Integrated systems for drug detection based on a multisensor approach including THz spectroscopy are currently installed at the Narita Airport in Tokyo to inspect all incoming airmail envelopes.[35] A challenging vision for THz-TDS systems would be to detect suspicious substances carried underneath someone's clothes. In principle, THz radiation is well suited for that application. THz waves are capable of penetrating dielectrics, such as clothes or plastic bags, and have a much better focusing ability than millimeter waves. In this scenario, the THz pulses are reflected at the surface of the substance carrying the spectroscopic information. After the detection, comparison with a database could identify a potential threat. But in real-world applications, this scenario is hampered by water vapor absorption (limited bandwidth), moving target (sliding focus), and long data acquisition time (small number of data points) which still requires intense engineering and data analysis.[36]

As a first step to approach this task, a database of signatures of commercial-grade explosives is needed. The Kramers–Kronig relation connects transmission absorption features to signatures in the reflectivity of the sample. Therefore, data of solid explosives in the transmission geometry are important. The measured absorption coefficients for some relevant explosives are plotted in Figure 12. The commercial-grade explosives RDX, PETN, and HMX have distinguishable features. For example, RDX has a prominent absorption peak at 0.82 THz.[37] Decision criteria for the particular substance are defined by a multispectral data analysis.[33]

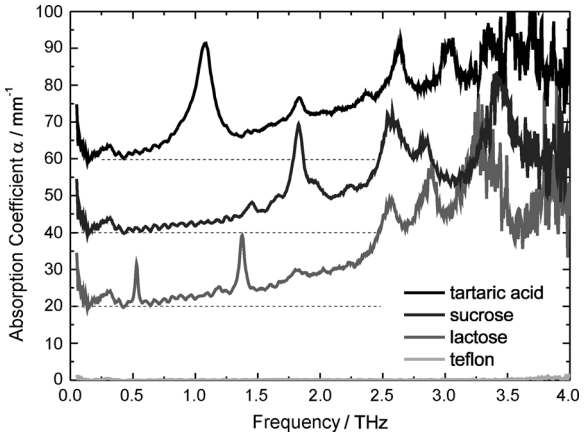

Figure 11. Absorption features of solids measured in transmission. The diluted pressed pellets containing molecular samples show a distinguishable signature in the THz range whereas the Teflon does not. Dashed lines indicate offset for clarity.

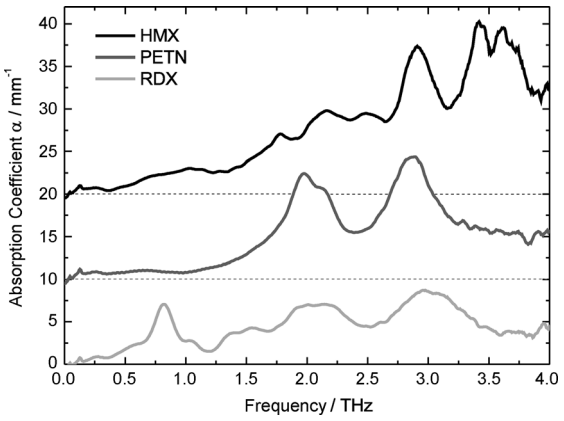

Figure 12. Absorption features of common explosives measured in transmission. The diluted pressed pellets show a distinguishable signature in the THz range. Dashed lines indicate offset for clarity.

 © 2011 Wiley-VCH Verlag GmbH & Co. KGaA, Weinheim

Various computational molecular modeling algorithms have been tested to assign observed absorption frequencies of a crystal to particular crystal modes (such as bending modes or phonons).[38] This is still challenging, especially for large molecules, but also shows possibilities to investigate and distinguish polymorphs of the same molecule by THz radiation.[39]

A complementary approach to the standard freely propagating THz-TDS has been that of using guided THz waves. Guided waves offer better sample detection sensitivity due to confinement of THz radiation within sub-wavelength gaps over a long interaction length. Increased detection sensitivity translates to a sub-milligram sample quantity required for characterization. There have been many earlier demonstrations of application of waveguides for performing sensitive spectroscopy at THz frequencies. Sprik et al.[40] employed sub-picosecond THz pulses propagating on coplanar transmission lines to measure magnetic resonances of an inorganic sample. More recently, Walther et al.[41] used free-space THz pulses coupled to a single metal wire transmission line to characterize vibrational modes of lactose. A third example was demonstrated by Byrne et al.,[42] who used the evanescent wave above a micro-strip transmission line to measure the 0.53 THz vibrational absorption line for a sub-milligram quantity of polycrystalline lactose that spatially overlapped the evanescent wave. These examples demonstrated the capability of the waveguide technique to characterize very small quantities of analyte sample.

The development of a good spectroscopic technique using a waveguide has the primary requirement based on a good waveguide geometry that supports distortion-free and dispersion-free THz pulse propagation. Mendis and Grischkowsky[43] have demonstrated that metal parallel-plate waveguides (PPWGs) support low-loss, dispersion-free, and distortion-free propagation of the lowest-order transverse magnetic mode (TM_0 = TEM mode). This, and the fact that the PPWG plates offer a nice flat metallic surface for sample deposition, makes them excellent choices for adaptation to perform sensitive spectroscopy. In fact this capability was demonstrated by Zhang and Grischkowsky[44] by applying these metal PPWGs to detect nanometer water layers within a 50 μm gap, Si-lens-coupled copper PPWG.

The researchers at Oklahoma State University in collaboration with the Naval Research Laboratories have very recently shown the application of these metal PPWGs to characterize polycrystalline thin films of molecules cast on metal plates comprising the PPWGs (see Figure 13). Using these single-mode metal PPWGs, molecular samples can be characterized with great sensitivity. It is shown that this technique yields much narrower linewidths of the THz vibrational modes in comparison to the standard pellet technique using a THz-TDS system, with linewidths rivaling single-crystal data. Using this method provides very narrow absorption resonances, which in turn yield much in depth understanding of the THz vibrational modes of the molecular solid. This technique was first applied to characterize 1,2-dicyanobenzene and tetracyanoquinodimethane.[45,46] Since then it has been widely applied to generalize the applicability to various molecules including organic, inorganic, biological, and explosive molecules. It has been shown that in each case the waveguide THz-TDS using metal PPWGs yielded substantially narrow resonance features along with the resolution of some features that were previously blurred by the limited resolution offered by standard THz (far-infrared) characterization techniques.[47–50]

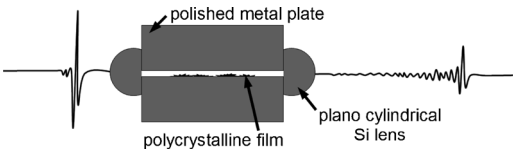

Figure 13. The metal parallel-plate waveguide assembly used for waveguide THz-TDS.

The PPWGs used for the measurement are fabricated from either aluminum, copper, or gold-coated copper. Both the plates have the dimensions of 27.9 mm (width) × 30.5 mm (length) × 9.5 mm (thickness). The inner surfaces were polished to a mirror finish. The PPWG assembly with a 50 μm gap was obtained by placing four metal spacers at the corners of each of the plates. THz pulses are coupled into and out of the PPWG using two plano-cylindrical Si lenses at the input and exit faces. An amplitude coupling efficiency of 20–25% is obtained for a PPWG with 50 μm gap. The sensitivity enhancement for such a PPWG is given by $\Gamma = L/n^3b$, where L is the length of the film, n is the refractive index of the film and b is the gap separation. Hence for a film with $n = 1.7$ and a waveguide with $b = 50$ μm and $L = 2.5$ cm, a sensitivity enhancement of 100 is predicted.[45]

As an example of the enhanced performance and line narrowing effect obtained using waveguide THz-TDS, 2,4-dinitrotoluene (2,4-DNT)[50] is characterized using both the standard pellet technique and the waveguide technique. The 2,4-DNT pellet was made from a uniform mixture of 32 mg of 2,4-DNT with 330 mg of polyethylene powder, and made into a pellet using a hydraulic press. 2,4-DNT films were obtained by drop-casting a solution (100 μL) of 2,4-DNT in acetone (2.5 mg mL^{-1}) on polished Al waveguide plates. The typical film mass was around 100 μg (almost 300 times less sample). The THz-TDS measurements were made as a function of temperature with the samples being cooled to 11 K using a He cryocooler. The absorbance amplitude of the pellet sample and the waveguide film is compared in Figure 14. Upon cooling to 11 K, the 2,4-DNT pellet revealed seven vibrational features with line centers and linewidths consistent with previous work. The narrowest linewidth was about 80 GHz. But when the waveguide film was cooled to 11 K we observed a dramatic resolution of 19 vibrational modes with two of those modes having a linewidth of 7 GHz. Nearly three times the number of lines observed with the pellet and ten times narrower linewidths are obtained with the waveguide THz-TDS technique, which corresponds to a substantial increase in both the obtainable information about the vibrational modes of this material and the precision of their identification.

The enhanced resolution obtained using the waveguide technique is attributed to the planar order of the polycrystalline film with respect to the metal surface. Figure 15 shows the

 © 2011 Wiley-VCH Verlag GmbH & Co. KGaA, Weinheim

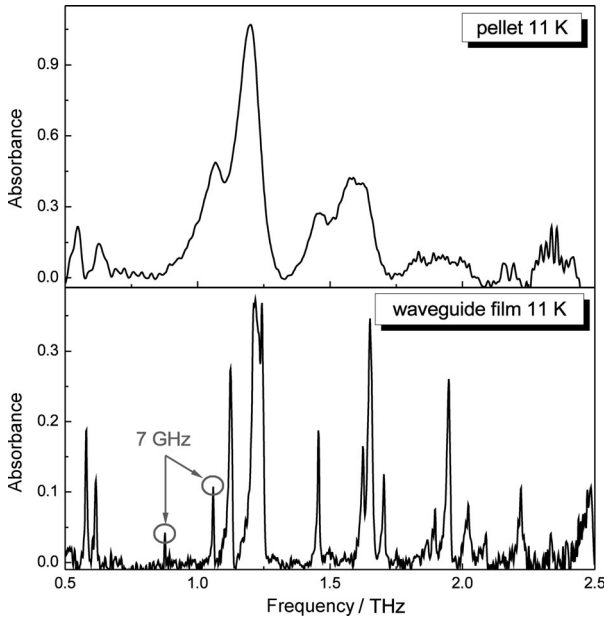

Figure 14. Enhanced resolution of the waveguide THz-TDS demonstrated by comparison of the vibrational data obtained from the pellet and waveguide film, measured at 11 K.

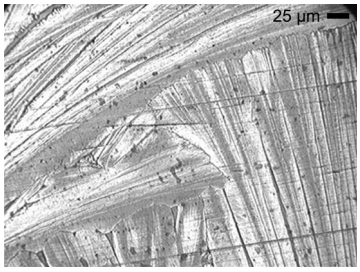

Figure 15. Optical micrograph of 2,4-DNT film on an Al waveguide plate.

optical micrograph of the 2,4-DNT film showing the planar oriented film. X-ray diffraction studies showed that the film had a strong preferential orientation on the (001) plane. 2,4-DNT is known to crystallize in the *P*21/*n* space group with eight molecules per unit cell.[51] The planar order of the polycrystalline film on the metal surface reduces the inhomogeneous broadening typically associated with pellet samples, which consist of randomly oriented microcrystals in the polymer matrix. Also, the sample film is expected be made up of microcrystals of higher crystalline quality, which is easier to make in comparison to single-crystal samples. In addition, the polycrystalline films are in direct contact with the metal plate and are hence expected to cool much more efficiently to the desired temperature, unlike the polymer pellets. Pellets contribute to inhomogeneous broadening arising from random stresses associated with pellet preparation. These improvements in sample quality and sample environment result in an enhancement in line resolution and facilitate the measurement of high-resolution vibrational spectra of most solid samples. This waveguide technique can be applied along with standard THz-TDS and FTIR techniques to obtain complete vibrational information of the desired sample.

5. Spectroscopic Imaging

It has been explained so far what type of features can be detected by using THz radiation. But all of the presented spectra were recorded in a single scan at one position of the sample. However, objects where the substance under investigation is distributed over a large area have to be scanned across the relevant region. So a complete THz image has to be recorded. As the development of multipixel THz systems with spectroscopic capabilities is still an ongoing process,[52] we will introduce a technique relying on the rapid scanning of one pixel and a relative movement of the object, the so-called raster scanning imaging.

To achieve a faster scanning speed the standard system was improved concerning the delay line and the data acquisition. The stepper-motor-driven delay line was upgraded with a shaker with a sinusoidal movement and a reduced scanning window of maximum 150 ps but having a repetition rate of 20 Hz. Scans for the back and forth movement enabled acquisition at a repetition rate of 40 Hz. The slow but high-resolution data acquisition hardware was replaced by a fast A/D card, so much more pixels could be recorded in a reasonable time with still good SNR. To demonstrate this possibility, a letter bomb mockup was made and raster scanned (Figure 16). It consisted

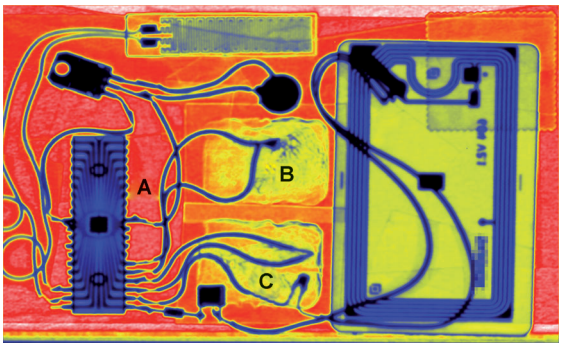

Figure 16. THz transmission through a mockup of a letter bomb. Various wirings, RFID chip, stamp, and suspicious bags are resolved.

of a paper envelope (A) containing a couple of electronics, a radio-frequency identification (RFID) chip, and two bags containing powder (B, C). A THz amplitude transmission image through the closed envelope is shown in Figure 16.

The advantage of THz-TDS is that the spectral information is also available for each pixel. Spectral averaging considerably increases the SNR of the spectrum. Lateral averaging at different spots is even more advantageous than recording the same pixel more often, as artifacts caused by sample irregularities such as thickness and inhomogeneities are minimized. To illustrate this improvement a region of interest is placed on different areas of the image around position A (blank envelope, Figure 16). The single pixels have a rather noisy and modulated

 © 2011 Wiley-VCH Verlag GmbH & Co. KGaA, Weinheim

spectrum depending on the sample thickness. As the reference is taken at a spot on the blank envelope, the single pixel contains modulations due to multiple reflections and thickness inhomogeneities of the paper. By averaging over several pixels these artifacts can be removed. Also, the SNR and the bandwidth are improved by reducing statistical noise. This is shown in Figure 17, in which a single pixel and an average of 10, 100, and 1000 pixels are shown. Coming from 1 to 1000 pixels, clearly the high-frequency noise level of the spectra is reduced, thereby increasing the accessible bandwidth from 2.2 to 2.7 THz. Remaining modulations can be minimized by increasing the number of pixels even further.

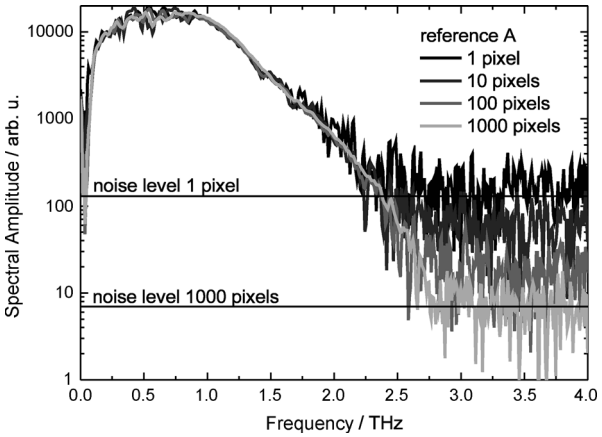

Figure 17. Single and multipixel references taken out of the data plotted in Figure 16 at position A. The bandwidth and SNR can be significantly improved by spatial averaging.

In Figure 18 the averages over 1000 pixels are shown for points A, B, and C. THz transmission clearly indicates absorption features at positions B and C. By choosing suitable regions of interest, the contents of positions B and C can be assigned to lactose (0.53, 1.20, 1.37, and 1.84 THz) and salicylic acid (1.13 and 1.42 THz). Despite the lateral inhomogeneity the features can be clearly resolved.

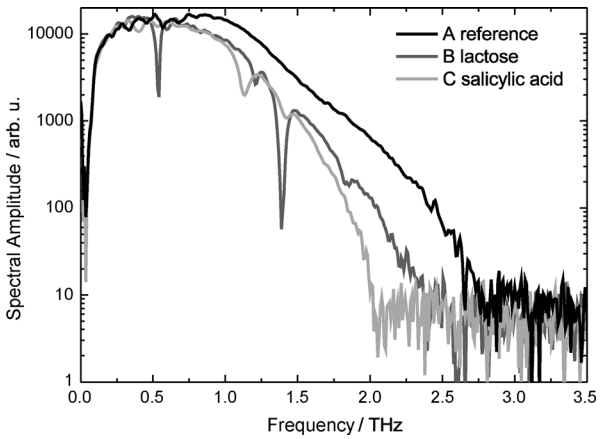

Figure 18. Spectral amplitude of 1000 averages taken at points A, B, and C in Figure 16. The signatures of the two bags (B, C) clearly show distinct absorption features, whereas the envelope (A) shows no signature.

In principle, this is a feasible application of broadband THz radiation. But still, the data acquisition time for the entire image is rather long (25 ms per pixel, hours of acquisition time in total). So the industrial implementation has to reduce the required number of data points by preselection or by using a sensor combination along with other imaging techniques. For example, an X-ray imager could make a preview of the envelope and thereby check for metal parts. Afterwards the suspicious areas could be scanned using THz radiation.

6. Time-of-Flight Information

A parameter that has not yet been explicitly evaluated is the phase of the pulse. A straightforward manifestation of the phase added by an inserted sample is the induced time delay. Let t_{sample} and t_{ref} be respectively the time delay of the sample and reference pulse, for example, the temporal position of the peak maximum. Then the time delay between these two pulses Δt is proportional to the sample thickness D [Eq. (5)]:

$$\Delta t = t_{sample} - t_{ref} = \frac{(n-1)}{c} D \quad (5)$$

with c the vacuum velocity of light and n the refractive index of the sample in the THz range. Typical refractive indices for example are 1.5 for common plastics or 3.4 for silicon. The refractive index n is either determined by measuring a sample of known thickness or by checking literature values. So through the evaluation of the pulse delay Δt caused by a sample with known refractive index n, the thickness D can be easily calculated. Depending on parameters such as the absorption of the sample, SNR of the THz system, and temporal stability of the measurement, layers down to a thickness of a few micrometers can be resolved in transmission.[53] Typical results are plotted in Figure 19, in which a stack of plastic wrap layers is measured. Each individual layer has a thickness of 12.5 μm at a refractive index of $n_{PE} = 1.5$.

The evaluation of the time delay, that is, the time delay of the pulse maximum or the zero crossing of the electric field

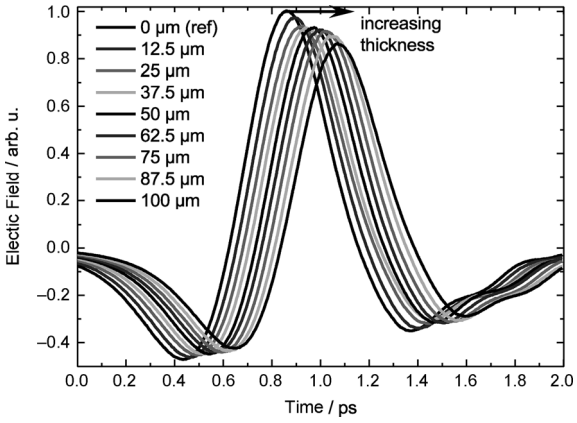

Figure 19. Measured THz pulse after propagation through plastic layers of varying thicknesses. The delay corresponding to the temporal shift of the pulses is directly proportional to the layer thickness.

 © 2011 Wiley-VCH Verlag GmbH & Co. KGaA, Weinheim

signal, gives a measure of the sample thickness (see Figure 20). A linear fit of the measured delay values indicates the high sensitivity of this measurement. This type of measurement is

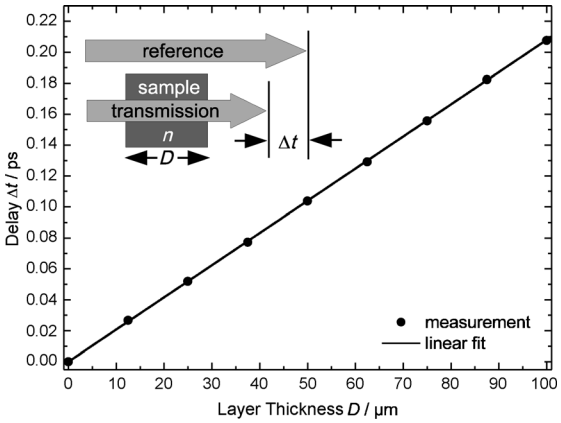

Figure 20. Evaluated pulse delay for the plastic layers in Figure 19. Inset: Experimental geometry of THz transmission measurement.

used for the nondestructive testing of, for example, styrofoam, plastics, and ceramics. Thickness deviations are resolved, and thereby air intrusions, impurities, or production failures can be detected. The layout of such a THz transmission measurement is shown in the inset of Figure 20.

A measurement geometry working in reflection is also possible. This is the case either if the sample is attached on a metal surface, where the THz pulse is reflected back completely, or at the interface between two media with any step of the refractive index n_1 and n_2, respectively. Then according to Fresnel's law, a fraction of the THz amplitude r is reflected at normal incidence [Eq. (6)]:

$$r = (n_1 - n_2)/(n_1 + n_2) \quad (6)$$

So at each interface with a refractive index step a reflection occurs. By evaluation of the delay (time of flight) a depth profile of the sample can be recorded. As a feasible application, the coating of multilayered tablets has been studied using pulsed THz radiation.[54] A complete mapping of multilayered coatings on tablets has been recorded by using reflection THz-TDS.[55] Even real 3D tomography of extended objects can be carried out in the THz range,[56] but always limited to nonconducting dry samples.

7. Summary and Outlook

In summary, we have discussed the possibilities and limitations of THz-TDS. By using broadband THz radiation, spectroscopic investigations of gases, liquids, and solids have been presented. For gases, the identification of polar molecules is possible, by probing narrowband rotational transitions. The limitations caused by the strong water vapor absorption were also investigated. For water molecules in the liquid phase, an ATR sensor was introduced to measure strongly absorbing samples. For solids, crystal modes can be probed in the THz range. Free-space measurements on molecular solids are presented. The obtained linewidth is improved considerably using PPWGs. Features as narrow as 7 GHz can be resolved. The available techniques have capabilities in various fundamental and industrial applications. Regarding the promising spectroscopic results, it is expected that this spectral range has the potential to become an additional tool to extend the scope of established infrared spectroscopy, also introducing features specific for the THz range itself.

Keywords: laser spectroscopy · rotational spectroscopy · sensors · time-resolved spectroscopy · vibrational spectroscopy

[1] W. L. Chan, J. Deibel, D. M. Mittleman, *Rep. Prog. Phys.* **2007**, *70*, 1325.
[2] D. Mansfield, E. Horlbeck, C. Bennett, R. Chouinard, *Int. J. Infrared Millimeter Waves* **1985**, *6*, 867.
[3] J. Faist, F. Capasso, D. L. Sivco, C. Sirtori, A. L. Hutchinson, A. Y. Cho, *Science* **1994**, *264*, 553.
[4] S. Matsuura, M. Tani, K. Sakai, *Appl. Phys. Lett.* **1997**, *70*, 559.
[5] K. Kawase, J.-I. Shikata, H. Ito, *J. Phys. D* **2002**, *35*, R1.
[6] D. Molter, M. Theuer, R. Beigang, *Opt. Express* **2009**, *17*, 6623.
[7] D. Grischkowsky, S. Keiding, M. Exter, C. Fattinger, *J. Opt. Soc. Am. B* **1990**, *7*, 2006.
[8] K. Cooper, R. Dengler, G. Chattopadhyay, E. Schlecht, J. Gill, A. Skalare, I. Mehdi, P. Siegel, *IEEE Microwave Wireless Components Lett.* **2008**, *18*, 64.
[9] M. van Exter, D. Grischkowsky, *IEEE Trans. Microwave Theory Tech.* **1990**, *38*, 1684.
[10] H. Harde, N. Katzenellenbogen, D. Grischkowsky, *J. Opt. Soc. Am. B* **1994**, *11*, 1018.
[11] D. H. Auston, *Appl. Phys. Lett.* **1975**, *26*, 101.
[12] P. Jepsen, R. Jacobsen, S. Keiding, *J. Opt. Soc. Am. B* **1996**, *13*, 2424.
[13] X.-C. Zhang, B. B. Hu, J. T. Darrow, D. H. Auston, *Appl. Phys. Lett.* **1990**, *56*, 1011.
[14] C. Weiss, R. Wallenstein, R. Beigang, *Appl. Phys. Lett.* **2000**, *77*, 4160.
[15] J. L'huillier, G. Torosyan, M. Theuer, Y. Avetisyan, R. Beigang, *Appl. Phys. B* **2007**, *86*, 185.
[16] J. L'huillier, G. Torosyan, M. Theuer, C. Rau, Y. Avetisyan, R. Beigang, *Appl. Phys. B* **2007**, *86*, 197.
[17] A. Nahata, D. H. Auston, T. F. Heinz, C. Wu, *Appl. Phys. Lett.* **1996**, *68*, 150.
[18] F. Ellrich, T. Weinland, M. Theuer, J. Jonuscheit, R. Beigang, *Tech. Mess.* **2008**, *75*, 14.
[19] R. A. Cheville, D. Grischkowsky, *Opt. Lett.* **1995**, *20*, 1646.
[20] M. Exter, C. Fattinger, D. Grischkowsky, *Opt. Lett.* **1989**, *14*, 1128.
[21] S. Wohnsiedler, M. Theuer, M. Herrmann, S. Islam, J. Jonuscheit, R. Beigang, F. Hase, *Proc. SPIE* **2009**, *7215*, 72150H.
[22] C. Weiss, E. Viehl, C. Theiss, G. Torosyan, M. Weinacht, R. Beigang, R. Wallenstein, *Tech. Mess.* **2001**, *68*, 388.
[23] A. Bartels, R. Cerna, C. Kistner, A. Thoma, F. Hudert, C. Janke, T. Dekorsy, *Rev. Sci. Instrum.* **2007**, *78*, 035107.
[24] G. Klatt, R. Gebs, C. Janke, T. Dekorsy, A. Bartels, *Opt. Express* **2009**, *17*, 22847.
[25] G. Klatt, R. Gebs, H. Schäfer, M. Nagel, C. Janke, A. Bartels, T. Dekorsy, *IEEE J. Sel. Top. Quantum Electron.* **2011**, *17*, 159.
[26] J. Pedersen, S. Keiding, *IEEE J. Quantum Electron.* **1992**, *28*, 2518.
[27] J. Kindt, C. Schmuttenmaer, *J. Phys. Chem.* **1996**, *100*, 10373.
[28] L. Thrane, R. Jacobsen, P. U. Jepsen, S. Keiding, *Chem. Phys. Lett.* **1995**, *240*, 330.
[29] T. T. L. Kristensen, W. Withayachumnankul, P. U. Jepsen, D. Abbott, *Opt. Express* **2010**, *18*, 4727.
[30] D. Banerjee, W. von Spiegel, M. D. Thomson, S. Schabel, H. G. Roskos, *Opt. Express* **2008**, *16*, 9060.
[31] F. M. Mirabella, *Appl. Spectrosc. Rev.* **1985**, *21*, 45.
[32] A. Dobroiu, R. Beigang, C. Otani, K. Kawase, *Appl. Phys. Lett.* **2005**, *86*, 261107.
[33] K. Kawase, Y. Ogawa, Y. Watanabe, H. Inoue, *Opt. Express* **2003**, *11*, 2549.

 © 2011 Wiley-VCH Verlag GmbH & Co. KGaA, Weinheim

[34] M. Leahy-Hoppa, M. Fitch, R. Osiander, *Anal. Bioanal. Chem.* **2009**, *395*, 247.
[35] H. Hoshina, Y. Sasaki, A. Hayashi, C. Otani, K. Kawase, *Appl. Spectrosc.* **2009**, *63*, 81.
[36] Y. Watanabe, K. Kawase, T. Ikari, H. Ito, Y. Ishikawa, H. Minamide, *Appl. Phys. Lett.* **2003**, *83*, 800.
[37] C. Konek, J. Wilkinson, O. Esenturk, E. Heilweil, M. Kemp, *Proc. SPIE* **2009**, *7311*, 73 110K.
[38] C. T. Konek, B. P. Mason, J. P. Hooper, C. A. Stoltz, J. Wilkinson, *Chem. Phys. Lett.* **2010**, *489*, 48.
[39] C. Strachan, P. Taday, D. Newnham, K. Gordon, J. Zeitler, M. Pepper, T. Rades, *J. Pharm. Sci.* **2005**, *94*, 837.
[40] R. Sprik, I. N. Duling, C.-C. Chi, D. Grischkowsky, *Appl. Phys. Lett.* **1987**, *51*, 548.
[41] M. Walther, M. R. Freeman, F. A. Hegmann, *Appl. Phys. Lett.* **2005**, *87*, 261107.
[42] M. B. Byrne, J. Cunningham, K. Tych, A. D. Burnett, M. R. Stringer, C. D. Wood, L. Dazhang, M. Lachab, E. H. Linfield, A. G. Davies, *Appl. Phys. Lett.* **2008**, *93*, 182904.
[43] R. Mendis, D. Grischkowsky, *Opt. Lett.* **2001**, *26*, 846.
[44] J. Zhang, D. Grischkowsky, *Opt. Lett.* **2004**, *29*, 1617.
[45] J. S. Melinger, N. Laman, S. S. Harsha, D. Grischkowsky, *Appl. Phys. Lett.* **2006**, *89*, 251110.
[46] J. S. Melinger, N. Laman, S. S. Harsha, S. Cheng, D. Grischkowsky, *J. Phys. Chem. A* **2007**, *111*, 10977.
[47] N. Laman, S. S. Harsha, D. Grischkowsky, J. S. Melinger, *Biophys. J.* **2008**, *94*, 1010.
[48] N. Laman, S. S. Harsha, D. Grischkowsky, *Appl. Spectrosc.* **2008**, *62*, 319.
[49] J. S. Melinger, N. Laman, D. Grischkowsky, *Appl. Phys. Lett.* **2008**, *93*, 011102.
[50] N. Laman, S. S. Harsha, D. Grischkowsky, J. S. Melinger, *Opt. Express* **2008**, *16*, 4094.
[51] W. McCrone, S. Tsang, *Anal. Chem.* **1954**, *26*, 1848.
[52] B. Pradarutti, R. Müller, W. Freese, G. Matthäus, S. Riehemann, G. Notni, S. Nolte, A. Tünnermann, *Opt. Express* **2008**, *16*, 18443.
[53] M. Theuer, R. Beigang, D. Grischkowsky, *Appl. Phys. Lett.* **2010**, *97*, 071106.
[54] A. Fitzgerald, B. Cole, P. Taday, *J. Pharm. Sci.* **2005**, *94*, 177.
[55] J. Zeitler, Y. Shen, C. Baker, P. Taday, M. Pepper, T. Rades, *J. Pharm. Sci.* **2007**, *96*, 330.
[56] K. Kawase, T. Shibuya, S. Hayashi, K. Suizu, *C. R. Phys.* **2010**, *11*, 510.

Received: February 28, 2011
Published online on July 6, 2011

 © 2011 Wiley-VCH Verlag GmbH & Co. KGaA, Weinheim